

# **Quasi-biennial oscillations of ozone and its implications in atmospheric dynamics and climate stability.**

MATHEMATICAL INSTITUTE, UNIVERSITY OF OXFORD

C5.11 Mathematical Geoscience

Candidate number: 1077723

Date: January 14, 2024

---

**Abstract.** The quasi-biennial oscillation (QBO) is one of the most predictable modes of large-scale internal variability in the Earth's atmosphere. We explore the effect of coupling a 1D model of the QBO winds to linearised equations of ozone radiation and photochemistry. We give a detailed description of the model and highlight the importance of incorporating the ozone feedback to obtain realistic results. In particular, it is found that including the ozone feedback smoothens the asymmetry between westerly and easterly winds, increases the zonal mean temperature, strengthens the ozone phase shift in the upper stratosphere, and drives ozone and upwelling perturbations in the lower stratosphere. Finally, we showcase how the ozone feedback mechanisms can stabilise the QBO in the face of an anthropogenic increase in carbon dioxide concentrations by reducing the percentual change in the QBO period as carbon dioxide levels rise.

---

## 1 Introduction

The quasi-biennial oscillation (QBO) [1, 2] consists of alternating layers of easterly and westerly<sup>1</sup> wind regimes that descend through the tropical stratosphere from near the stratopause down to the tropopause at approximately 1km per month. It has a variable period averaging to 28 months (about two years), hence its name.

Other than the fluctuations associated with seasonal cycles and diurnal changes, the QBO is one of the most predictable modes of large-scale internal variability<sup>2</sup> in the Earth's atmosphere. Moreover, although the QBO is a tropical phenomenon, it influences atmospheric processes all over the globe [2] such as the stratospheric polar vortex, subtropical jets, semi-annual oscillations in the stratosphere and mesosphere, etc. Therefore, simulating the QBO and its teleconnections accurately is crucial to making better climate and weather forecasts.

For this purpose, an understanding of the influence of the QBO not only on zonal wind but also on temperature and the distribution of trace species is essential. The QBO changes in stratospheric circulation affect temperature patterns by creating anomalies to maintain thermal wind balance. At the same time, the QBO influences the distribution of stratospheric trace gases and aerosols. In particular, stratospheric ozone exhibits a strong QBO signal. Since the ozone mixing ratio exhibits a vertical gradient, the QBO-induced vertical motion drives the transport of ozone due to vertical advection. At the same time, since ozone is a greenhouse gas — that is, it absorbs radiation — changes in its concentration feedback onto the temperature and, therefore, the QBO's period and amplitude.

Recently, there have been unforeseen disruptions of the QBO [3]. While the exact causes are not yet fully understood, these disturbances are believed to be partially due to the ongoing trend of warming climate. Further, given that ozone is a greenhouse gas, any changes in its distribution due to QBO disruptions could potentially worsen the climate situation. This project aims to explore the influence of ozone feedback on the dynamics of the QBO amidst the backdrop of climate change.

---

<sup>1</sup>*Easterlies* and *westerlies* refer to winds blowing from the east and west respectively. These terms are equivalent to *westward* and *eastward* winds respectively.

<sup>2</sup>Variability refers to aspects of the climate deviating from their long-term averages.

Symbol	Description	Value	Reference
$\kappa$	Vertical diffusion	$0.30 \text{ m}^2 \text{s}^{-1}$	[4]
$F$	Wave momentum flux	$1.60 \times 10^{-2} \text{ m}^2 \text{s}^{-2}$	[4]
$N$	Buoyancy frequency	$2.16 \times 10^{-2} \text{ s}^{-1}$	[4]
$\mu$	Thermal dissipation rate	$1.00 \times 10^{-6} \text{ s}^{-1}$	[4]
$\alpha$	Damping coefficient	eq. (10)	[4]
$k$	Wavenumber	$2\pi/(40 \times 10^6) \text{ m}^{-1}$	[4]
$c$	Phase speed	$30.0 \text{ m s}^{-1}$	[4]
$H$	Density scale height	$7.00 \times 10^3 \text{ m}$	[4, 5]
$\Omega$	Earth rotation rate	$7.27 \times 10^{-5} \text{ m s}^{-1}$	—
$a$	Earth radius	$6.37 \times 10^6 \text{ m}$	—
$\beta$	Rossby parameter	$2\Omega/a$	—
$L$	QBO's meridional scale	$1.00 \times 10^6 \text{ m}$	[5]
$R$	Dry air gas constant	$287 \text{ m}^2 \text{s}^{-2} \text{K}^{-1}$	—
$h$	Newtonian cooling coefficient	eq. (22)	[6]*
$\gamma_O$	Ozone photochemical coefficient	$1.80 \times 10^{-7} \text{ s}^{-1}$	[5]
$\gamma_T$	Temperature photochemical coefficient	$-9.00 \times 10^{-13} \text{ m}^{-1} \text{s ppv}$	[5]
$s_O$	Ozone heating coefficient	$8.32 \times 10^{-2} \text{ m s}^{-3} \text{ ppv}^{-1}$	[5]
$s_C$	Aerosol heating coefficient	$-1.00 \times 10^{-7} \text{ m s}^{-3} \text{ ppv}^{-1}$	—

**Table 1:** Numerical values of the model’s parameters. The asterisk means that the coefficient was modified from what was given by the source. In this case, it was reduced by two orders of magnitude as discussed in section 2.2.

## 2 Model Description

In this section, we present a one-dimensional model in which the average zonal-mean wind  $\bar{u}$ , temperature  $\bar{T}$  and ozone mixing ratio  $\chi_O$  are only functions of height  $z \in [z_l, z_t]$  and time  $t \geq 0$ . An overview of all the parameters used is given in table 1.

### 2.1. ZONAL WIND

The QBO [1, 2] is an oscillating mean flow driven by the two-way feedback interaction between the background stratospheric winds and vertically propagating tropospheric equatorial waves. Its basic mechanism [1, 2], illustrated in fig. 1, works as follows.

Consider a background stratospheric flow  $\bar{u}(z)$  — that is, the wind in the absence of waves — in the latitudinal direction (x-direction) which varies with height (z-direction). This flow is now perturbed by waves with horizontal phase speeds  $c_n$  propagating vertically with certain vertical group velocities. On one hand, background flow alters

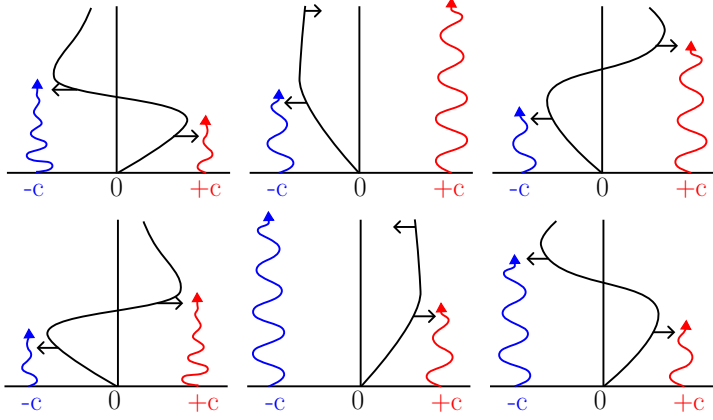


**Fig. 1:** Evolution of the zonal-mean wind  $\bar{u}$  (black line) forced by two upward propagating waves with the same amplitude and equal but opposite horizontal phase speeds  $\pm c$ . The horizontal and vertical axes are horizontal velocity and height  $z$  respectively. The wavy lines show the vertical penetration of westward (blue) and eastward (red) waves, with diminishing amplitude signifying dissipation as they traverse the stratosphere (they do not represent changes in phase speed). Black arrows represent momentum deposition when the  $\bar{u}$  approaches  $\pm c$ . Adapted from [1].

waves' momentum fluxes for, as they propagate vertically through the stratosphere, their vertical wavelength and vertical group velocity decrease as  $\bar{u}(z)$  approaches  $c_n$  with altitude. Wave dissipation – due to radiative damping, wave breaking, etc. – increases under these conditions and is maximised near critical layers where  $|\bar{u}(z) - c_n|$  is zero. At the same time, the waves' momentum fluxes alter the background flow. Dissipation leads to lateral momentum deposition by the waves that locally accelerate  $\bar{u}$  towards their phase speeds  $c_n$ . This acceleration is maximised as  $|\bar{u} - c_n|$  reaches zero and the waves with phase speed  $c_n$  are completely absorbed.

Hence, each wave undergoes the following cycle creating a pattern of descending winds: (a) the wave propagates until it reaches its critical layer, where it is fully absorbed; (b) acceleration of  $\bar{u}(z)$  by this wave predominantly occurs below this point, so  $\bar{u}(z)$  reaches  $c_n$  slightly earlier and the wind pattern descends; (c) the critical layer is reached at lower heights, so the wave is fully absorbed earlier; (d) the cycle repeats until the wave is fully absorbed at the lower boundary; (e) since this wave is not able to propagate through the stratosphere, the mean flow is accelerated by waves with other phase speeds, causing  $\bar{u}(z)$  to move away from  $c_n$  at the lower boundary; (f) the wave can now propagate to the top, marking the restart of the cycle.

While in reality the QBO is driven by a broad spectrum of waves, its fundamental behaviour is adequately captured by agglomerating all of them in two as shown in fig. 1. This is the approach we will take for the remainder of the project. These waves are generated by convection processes in the tropics and have sizes ranging from mesoscale (small-scale gravity waves) to planetary scales (global-scale Kelvin and Rossby-gravity waves). In this project, we will restrict ourselves to the latter, assuming they dominate wind perturbations like previously done in [4, 6, 7, 8]. In the following subsections, we will explore how this mechanism can be described mathematically.

### 2.1.1 Simple QBO Model

**Plumb Model.** Following the one-dimensional QBO model described in [7], the evolution of  $\bar{u}(z, t)$  obeys the equation

$$\frac{\partial \bar{u}(z, t)}{\partial t} = - \sum_n \frac{\partial F_n(z, t)}{\partial z} + \kappa \frac{\partial^2 \bar{u}(z, t)}{\partial z^2}. \quad (1)$$

The term on the left-hand side represents the rate of change of zonal-mean wind. The terms on the right-hand side represent wave momentum deposition and diffusion respectively. Here,  $\kappa$  is the vertical diffusion constant and  $F_n$  is the horizontal momentum flux associated with the n-th wave given by

$$F_n(z, t) = F_n(z_l) \exp \left( - \int_{z_l}^z \frac{N\mu}{k_n(\bar{u}(z', t) - c_n)} dz' \right). \quad (2)$$

$F_n(z_l)$  represents momentum deposition at the lower boundary, and the exponential term characterizes the attenuation of the wave as it traverses the stratosphere. The damping of the n-th wave is characterised by the thermal dissipation rate  $\mu$ , the buoyancy frequency  $N$ , its wavenumber  $k_n$ , and the difference between its phase speed  $c_n$  and  $\bar{u}$ . Hence, as we approach the critical layer ( $|\bar{u} - c_n| \rightarrow 0$ ) the wave flux drops to zero meaning that the wave has been absorbed by the mean flow and all its momentum deposited. Here,  $N^{-1}$  measures the response time of stratification to perturbations. A fast response to perturbations (bigger values of  $N$ ) leads to a more stable stratosphere where waves are more effectively damped. Equation (2) can be derived from the continuity, Navier-Stokes, and buoyancy equations by performing a Boussinesq approximation of the stratospheric flow and taking into account small

perturbations of velocity caused by waves. For an outline of this derivation, please refer to appendix A.

**Non-dimensionalisation.** Equations (1) and (2) may be non-dimensionalised by defining

$$\bar{u} = [c]\hat{u}, \quad c = [c]\hat{c}, \quad k_n = [k]\hat{k}_n, \quad N = [N]\hat{N}, \quad \mu = [\mu]\hat{\mu}, \quad F_n(z_l) = [F]\hat{F}_n(z_l), \quad (3)$$

$$\alpha = \frac{N\mu}{[N][\mu]}, \quad \Lambda = \frac{\kappa[N][\mu]}{[k][c][F]}, \quad (4)$$

where the characteristic scales are denoted by brackets and the non-dimensional constants by hats. If we then use the non-dimensional coordinates

$$\eta = \frac{[N][\mu]}{[k][c]^2}(z - 17\text{km}), \quad \xi = \frac{[N][\mu][F]}{[k][c]^3}t, \quad (5)$$

we arrive at the non-dimensional equations

$$\frac{\partial \bar{u}(\eta, \xi)}{\partial \xi} = - \sum_n \frac{\partial F_n(\eta)}{\partial \eta} + \Lambda \frac{\partial^2 \bar{u}(\eta, \xi)}{\partial \eta^2}, \quad (6)$$

$$F_n(\eta) = F_n(\eta_l) \exp\left(-\int_{\eta_l}^{\eta} g_n(\eta') d\eta'\right), \quad g_n(\eta) = \frac{\alpha}{k_n(\bar{u}(\eta, \xi) - c_n)^2}, \quad (7)$$

where the hats have been dropped and  $g_n$  is referred to as the attenuation rate and  $\alpha$  as the damping coefficient.

### 2.1.2 Extended QBO Model

**Density.** The approximation of the atmosphere as a Boussinesq fluid — that is, density is taken to be constant except when it gives rise to buoyancy forces — leads to the stratification of the mean flow being described solely in terms of  $N$ . This is not strictly valid as stratification significantly influences the vertical structure of momentum dissipation. Following [4, 6, 8], we can locally assume constant density while allowing it to vary with height giving

$$\frac{\partial \bar{u}(z, t)}{\partial t} = -\frac{\bar{\rho}(z_l)}{\bar{\rho}(z)} \sum_n \frac{\partial F_n(z, t)}{\partial z} + \kappa \frac{\partial^2 \bar{u}(z, t)}{\partial z^2}, \quad (8)$$

leaving  $F_n$  and  $g_n$  unchanged. Like [4] but unlike [8], we do not absorb  $\bar{\rho}(z_l)$  into  $F_n(z_l)$ . Since temperature variations are not too big in the stratosphere, we can assume it is isothermal giving an exponential mean density profile

$$\bar{\rho}(z) = \bar{\rho}(z_l) \exp\left(-\frac{z - z_l}{H}\right), \quad (9)$$

where  $H$  is the density scale height and the  $\bar{\rho}(z_l)$ 's in the fraction preceding of the forcing term of eq. (8) cancel. Note that this assumption does not prevent us from considering small temperature perturbations in the next subsection.

**Damping coefficient.** A constant damping coefficient is also not always a good approximation, and we can improve it by setting, like [4],

$$\alpha(z) = \begin{cases} 0.55 + 0.56 \left(\frac{z-17\text{km}}{6.5\text{km}}\right), & 17\text{km} \leq z \leq 30\text{km}, \\ 1.65, & z > 30\text{km}, \end{cases} \quad (10)$$

which can be written in terms of the non-dimensional variable  $\eta$  using eq. (5).

**Waves.** We can further improve the model by considering a more realistic forcing composed of an eastward Kelvin wave (subscript K) and a westward Rossby-gravity wave (subscript RG) by altering the rates of decay.

To do so we define the Coriolis frequency  $f = 2\Omega \sin \varphi$  and the Rossby parameter

$$\beta = \frac{1}{a} \frac{\partial f}{\partial \varphi} = \frac{2\Omega}{a} = [k]^2 [c] \hat{\beta}, \quad (11)$$

where  $\varphi$  is latitude,  $\Omega$  is the angular speed of the Earth's rotation,  $a$  is Earth's radius, and we used  $\varphi = 0$  since we are considering the QBO at the tropics. Now, following [8], we modify the attenuation rates to

$$g_K(\eta, \xi) = \frac{\alpha(\eta)}{k_K(\bar{u}(\eta, \xi) - c_K)^2}, \quad (12)$$

$$g_{RG}(\eta, \xi) = \frac{\alpha(\eta)}{k_{RG}(\bar{u}(\eta, \xi) - c_{RG})^2} \left[ \frac{\beta}{k_{RG}^2(\bar{u} - c_{RG})} - 1 \right], \quad (13)$$

where we dropped the hats and left out the temperature dependence shown in [8] to improve the stability of the numerical implementation. Conventionally, westerly

(eastward) velocities are positive and easterly (westward) velocities are negative, so  $c_K > 0$  and  $c_{RG} < 0$ . Moreover, Rossby-gravity waves' horizontal wavelengths are smaller those of Kelvin waves, so we set  $k_{RG} = 3k_K$ .

**Upwelling.** There is a global mass circulation pattern called the Brewer-Dobson circulation [9] in which air rises into the stratosphere at the tropics and moves polewards as it descends until it reaches middle-high latitudes. Following [4, 6, 10], we can expand the model by taking into account the effect of advection by the tropical branch of the Brewer-Dobson circulation through the inclusion of an upwelling term,

$$\frac{\partial \bar{u}(z, t)}{\partial t} + w \frac{\partial \bar{u}(z, t)}{\partial z} = -\exp\left(\frac{z - z_l}{H}\right) \sum_n \frac{\partial F_n(z, t)}{\partial z} + \kappa \frac{\partial^2 \bar{u}(z, t)}{\partial z^2}. \quad (14)$$

Here,  $w$  is the strength of upwelling. In the next subsection, we will explore a possible expression for this variable in terms of temperature and gas mixing ratios.

**Non-dimensionalisation.** Equation (14) can be non-dimensionalised by defining

$$\epsilon = \frac{1}{H} \frac{[N][\mu]}{[k][c]^2}, \quad w = \frac{[F]}{[c]} \hat{w}, \quad (15)$$

which leads to

$$\frac{\partial \bar{u}(\eta, \xi)}{\partial \xi} + w(\eta, \xi) \frac{\partial \bar{u}(\eta, \xi)}{\partial \eta} = -\exp[\epsilon(\eta - \eta_l)] \sum_n \frac{\partial F_n(\eta, \xi)}{\partial \eta} + \Lambda \frac{\partial^2 \bar{u}(\eta, \xi)}{\partial \eta^2}, \quad (16)$$

where the hats have been dropped. Note that in the limit where  $w, \epsilon \rightarrow 0$  we recover the Plumb model.

**Summary.** The non-dimensional extended QBO model is given by the zonal-mean wind evolution eq. (16), the wave momentum flux eq. (7), the damping coefficient eq. (10), the attenuation rates eqs. (12) and (13), and the upwelling equation that is yet to be defined. Once we get the non-dimensional solution we can get the dimensional height, time, zonal-mean wind, and upwelling from eqs. (3), (5) and (15).

## 2.2. TEMPERATURE AND OZONE

In this section, we will explore how the QBO perturbations in zonal-mean wind lead to perturbations in zonal-mean temperature and ozone mixing ratios. Further, we will examine how these perturbations contribute to feedback mechanisms within the QBO by influencing upwelling.

**Temperature:** The QBO exhibits a clear signature in temperature because it must be in thermal wind balance with the zonal winds. Thermal wind balance [11] describes the variation in wind patterns with height due to a horizontal temperature gradient, or vice-versa, due to geostrophic and hydrostatic balance. Geostrophic balance refers to the horizontal pressure gradient force being equilibrated by the Coriolis force. As wind moves from high to low-pressure ( $p$ ) areas, the Coriolis force ( $f_c$ ) deflects it to the right in the Northern and to the left in the Southern Hemisphere. This is described by

$$f_c u = -\frac{1}{\rho} \frac{\partial p}{\partial y}. \quad (17)$$

Hydrostatic balance refers to the vertical pressure gradient force being equilibrated by gravity. This can be described by

$$\rho g = -\frac{\partial p}{\partial z}. \quad (18)$$

Equations (17) and (18) can be equated after differentiating them with respect to  $z$  and  $y$  respectively. A relationship between temperature and  $u$  can be found assuming an equation of state like the ideal gas law. Doing so and integrating over the tropical latitudes in log-pressure coordinates as demonstrated in [12], the zonal-mean temperature deviation from the average is found to be

$$\bar{T}(z, t) = -\frac{L^2 \Omega H}{Ra} \frac{\partial \bar{u}(z, t)}{\partial z}, \quad (19)$$

where  $R$  is the gas constant for dry air and  $L$  is the meridional scale of the QBO. Hence, we expect cold anomalies near the tropopause associated with westerly phases — that is, easterly winds (negative  $\bar{u}$ ) in the lower atmosphere and westerly winds (positive  $\bar{u}$ ) in the mid-atmosphere, so  $\partial \bar{u} / \partial z > 0$  — and the opposite for easterly phases.

**Ozone:** Following [5, 6, 12], the continuity equation of ozone can be written as

$$\frac{\partial \chi_O(z, t)}{\partial t} + w(z, t) \frac{\partial \chi_O(z, t)}{\partial z} = \gamma_O \chi_O(z, t) + \gamma_T \frac{R\bar{T}(z, t)}{H}. \quad (20)$$

The terms on the left-hand side represent the rate of change in the ozone mixing ratio and upwelling. The terms on the right-hand side represent the damping of ozone perturbations through photochemical reactions. The photochemistry of ozone is linearised with respect to the ozone mixing ratio and temperature. Here,  $\chi_O$  is the ozone mixing ratio and  $\gamma_n$  the photochemical coefficients. Given that  $\gamma_T < 0$  (table 1), warm QBO temperature anomalies lead to a reduction in ozone concentrations, while cold QBO anomalies result in an increase.

**Upwelling:** Again following [5, 6, 12], we consider the impact of temperature and ozone anomalies in QBO winds through changes in the upwelling term. Vertical motion is described by balancing diabatic heating (or cooling) with adiabatic expansion (or compression) as follows,

$$w(z, t)N^2 = -h(z) \frac{R\bar{T}}{H} + s_O \chi_O(z, t) + s_C \chi_C(z, t). \quad (21)$$

The term on the left-hand side represents adiabatic expansion, wherein the warming of air induces upwelling, while the cooling of air results in sinking. The terms on the right-hand side represent diabatic heating. This includes infrared cooling by temperature anomalies and heating due to the absorption of solar radiation by ozone and carbon dioxide perturbations, respectively. Here,  $\chi_C$  is the carbon dioxide mixing ratio,  $s_n$  the heating coefficients, and  $h$  the Newtonian cooling coefficient

$$h(z) = \begin{cases} \left(1 + \frac{2}{3} \frac{z-17\text{km}}{6.5\text{km}}\right) \times 5.4 \times 10^{-9} \text{s}^{-1}, & 17\text{km} \leq z \leq 30\text{km}, \\ 1.56 \times 10^{-8} \text{s}^{-1}, & z > 30\text{km}. \end{cases} \quad (22)$$

This coefficient was taken from [6] and reduced by two orders of magnitude because, otherwise, upwelling was too strong for the QBO to form. This problem could be arising because we are not taking into account the temperature dependence of the attenuation rates in eqs. (12) and (13).

**Non-dimensionalisation.** Equations (19) to (21) can be non-dimentionalised setting

$$\bar{T} = \frac{L^2 \Omega H[N][\mu]}{Ra[k][c]} \hat{T}, \quad \chi_n = [\chi] \hat{\chi}_n, \quad (23)$$

$$\Gamma_O = \frac{\gamma_O[k][c]^3}{[\mu][F][N]}, \quad \Gamma_T = \frac{\gamma_T L^2 \Omega[c]^2}{a[F][\chi]}, \quad \Xi = \frac{h L^2 \Omega[\mu]}{a[k][F][N]}, \quad S_n = \frac{s_n[c][\chi]}{[F][N]^2}, \quad (24)$$

which leads to the non-dimensionalised

$$\bar{T}(\eta, \xi) = -\frac{\partial \bar{u}(\eta, \xi)}{\partial \eta}, \quad (25)$$

$$\frac{\partial \chi_O(\eta, \xi)}{\partial \xi} + w(\eta, \xi) \frac{\partial \chi_O(\eta, \xi)}{\partial \eta} = \Gamma_O \chi_O(\eta, \xi) + \Gamma_T \bar{T}(\eta, \xi), \quad (26)$$

$$w(\eta, \xi) = -\Xi(\eta) \bar{T}(\eta, \xi) + S_O \chi_O(\eta, \xi) + S_C \chi_C(\eta, \xi). \quad (27)$$

Hence, we can use eqs. (25) to (27) to update temperature, ozone concentration and upwelling strength respectively. Once we get the non-dimensional solution we can get the dimensional temperature and mixing ratios from eq. (23).

**Summary.** The complete QBO model is given by the zonal-mean wind evolution eq. (16), the wave momentum flux eq. (7), the damping coefficient eq. (10), the attenuation rates eqs. (12) and (13), the temperature eq. (25), the ozone continuity eq. (26), and the upwelling eq. (27). Once we get the non-dimensional solution we can get the dimensional height, time, zonal-mean wind, upwelling, temperature, and mixing ratios from eqs. (3), (5), (15) and (23). This system of equations can be discretised and integrated numerically as we will see in the following section.

### 3 Numerical Implementation

In this section, we describe the semi-implicit finite difference scheme used to solve the extended QBO model with temperature and ozone contributions. To integrate the simple QBO model, we follow the same scheme setting  $w$  and  $\epsilon$  to zero.

We define a domain covering 5000 days and roughly the extension of the stratosphere from the tropopause at 17km to near the stratopause at 43km from the surface.

$$\{(z, t) \in ([17, 43]\text{km} \times [0, 5000]\text{days})\}, \quad (28)$$

This domain is then non-dimentionalised and discretised as follows

$$\{(\eta_j, \xi_n) := (j\Delta\eta, n\Delta\xi) \in ([0, 4] \times [0, 44]) : j = 0, 1, \dots, J \text{ and } n = 0, 1, \dots, N\}, \quad (29)$$

where  $J = 100$  and  $N = 10^5$ . Hence, the stepsize is  $\Delta\eta = 0.04$  (0.26 km) and timestep is  $\Delta\xi = 4.4 \times 10^{-4}$  (0.05 days).

Now, we integrate over time using a semi-implicit finite differences scheme where the non-linearities are calculated explicitly. The basic procedure at timestep  $n + 1$ , given the previous state at  $n$  is as follows. Firstly, we calculate the momentum flux term of eq. (16) explicitly,

$$G(\eta_j, \xi_{n+1}) = -\exp(\epsilon\eta_j) \sum_i \frac{\partial F_i(\eta_j, \xi_n)}{\partial \eta}. \quad (30)$$

Care must be taken with this term as it tends to infinity as  $\bar{u} \rightarrow c_i$ . Hence, we impose the condition that  $G(\eta_j, \xi_{n+1}) < 100$  and set it to 100 if this limit is exceeded. Secondly, we update the approximation  $\bar{U}_j^{n+1}$  of  $\bar{u}(\eta_j, \xi_{n+1})$  using an implicit Euler scheme for eq. (16).

$$\frac{\bar{U}_j^{n+1} - \bar{U}_j^n}{\Delta\xi} + W_j^n \frac{\bar{U}_j^{n+1} - \bar{U}_{j-1}^{n+1}}{\Delta\eta} = G(\eta_j, \xi_{n+1}) + \Lambda \frac{\bar{U}_{j+1}^{n+1} - 2\bar{U}_j^{n+1} + \bar{U}_{j-1}^{n+1}}{(\Delta\eta)^2}, \quad (31)$$

for  $n = 0, 1, \dots, N - 1$  and  $j = 1, 2, \dots, J - 1$  with

$$\bar{U}_0^{n+1} = 0, \quad n = 0, 1, \dots, N - 1, \quad (32)$$

$$\frac{\bar{U}_{J-2}^{n+1} - 4\bar{U}_{J-1}^{n+1} + 3\bar{U}_J^{n+1}}{2\Delta\eta} = 0, \quad n = 0, 1, \dots, N - 1, \quad (33)$$

$$\bar{U}_j^0 = 0.5 \sin\left(\frac{\pi j \Delta\eta}{4}\right), \quad j = 0, 1, \dots, J, \quad (34)$$

where eqs. (32) and (33) correspond to setting Dirichlet ( $\bar{u}(0, \xi) = 0$ ) and Neumann ( $\partial_z \bar{u}(4, \xi) = 0$ ) boundary conditions respectively and eq. (34) corresponds to setting initial condition  $\bar{u}(\eta, 0) = 0.5 \sin(\pi\eta/4)$ . Thirdly, we update the approximation  $\tilde{T}_j^{n+1}$

of  $\bar{T}(\eta_j, \xi_{n+1})$  evaluating eq. (25) using finite differences.

$$\tilde{\bar{T}}_j^{n+1} = -\frac{\bar{U}_{j+1}^{n+1} - \bar{U}_{j-1}^{n+1}}{2\Delta\eta}, \quad j = 1, 2, \dots, J-1, \quad (35)$$

$$\tilde{\bar{T}}_0^{n+1} = \frac{-3\bar{U}_0^{n+1} + 4\bar{U}_1^{n+1} - 1\bar{U}_2^{n+1}}{2\Delta\eta}, \quad \tilde{\bar{T}}_J^{n+1} = \frac{\bar{U}_{J-2}^{n+1} - 4\bar{U}_{J-1}^{n+1} + 3\bar{U}_J^{n+1}}{2\Delta\eta} \quad (36)$$

This doesn't require any boundary conditions. Fourthly, we update approximation  $(X_O)_j^{n+1}$  of  $\chi_0(\eta_j, \xi_{n+1})$  using an upwind implicit scheme for eq. (26). Extra care must be taken when building this scheme as it will change depending on the sign of the upwelling term.

$$\begin{aligned} \frac{(X_O)_j^{n+1} - (X_O)_j^n}{\Delta\xi} + [W_j^n]^+ \frac{(X_O)_j^{n+1} - (X_O)_{j-1}^{n+1}}{\Delta\eta} \\ + [W_j^n]^- \frac{(X_O)_{j+1}^{n+1} - (X_O)_j^{n+1}}{\Delta\eta} = \Gamma_O(X_O)_j^{n+1} + \Gamma_T \tilde{\bar{T}}_j^{n+1}, \end{aligned} \quad (37)$$

for  $n = 0, 1, \dots, N-1$  and  $j = 1, 2, \dots, J-1$ . This is also the case for the boundary conditions but not for the initial condition.

$$\bar{X}_0^{n+1} = 0, \quad n = 0, 1, \dots, N-1, \text{ if } W_0^n > 0, \quad (38)$$

$$\frac{X_{J-2}^{n+1} - 4X_{J-1}^{n+1} + 3X_J^{n+1}}{2\Delta\eta} = 0, \quad n = 0, 1, \dots, N-1, \text{ if } W_J^n < 0, \quad (39)$$

$$X_j^0 = 0.01 \sin\left(\frac{\pi j \Delta\eta}{2}\right), \quad j = 0, 1, \dots, J, \quad (40)$$

where  $[.]^\pm$  refers to the positive and negative parts of the term inside the brackets. Again, eqs. (38) and (39) set (if needed) Dirichlet and Neumann boundary conditions at the bottom and at the top respectively and eq. (40) corresponds to setting initial condition  $\chi_0(\eta, 0) = 0.25 \cos(\pi\eta/4)$ . Finally, we update the approximation  $W_j^{n+1}$  of  $w(\eta_j, \xi_{n+1})$  summing up the terms in eq. (27).

$$W_j^{n+1} = -\Xi(\eta_j) \tilde{\bar{T}}_j^{n+1} + S_0(X_O)_j^{n+1} + S_C \chi_C(\eta_j), \quad (41)$$

for  $n = 0, 1, \dots, N-1$  and  $j = 0, \dots, J$ .

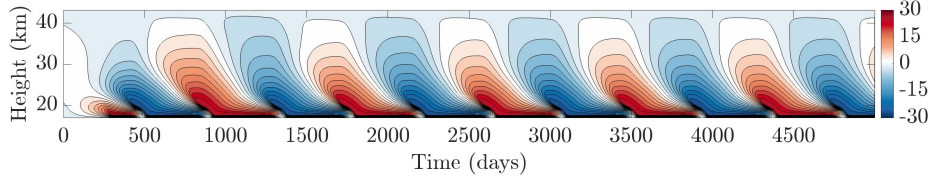


**Fig. 2:** Time-height sections of the QBO component of the zonal-mean wind (m/s) calculated integrating eqs. (6) and (7). The period was found to be 28.42 months.

## 4 Results

In this section, we present the results of numerically integrating the QBO model. The numerical values of the parameters used are given in table 1. Throughout this section, the period of the QBO was found by calculating the auto-correlation function of the zonal-mean wind at  $z = 24\text{km}$  and estimating the average distance between its peaks.

### 4.1. QBO MECHANISM

In this subsection, we will explore the differences between the simple and the extended QBO model. For simplicity and better understanding, we will drop the upwelling terms until the next section.

**Simple QBO model.** The result of numerically integrating the simple QBO model is given in fig. 2. It clearly captures the basic characteristics of the QBO with descending patterns of westerly and easterly winds of up to  $30\text{m s}^{-1}$  and a period of around 28 months. The westerly and easterly phases are completely symmetric. Note that it takes some days for the influence of the initial conditions to disappear and the QBO phases to become indistinguishable from the ones before or after (visibly around one to two cycles).

**Extended QBO model.** The result of numerically integrating the extended QBO model without upwelling ( $h = 0$ ,  $s_O = 0$ ,  $s_C = 0$ ) is given in fig. 3. It exhibits zonal wind oscillations similar to fig. 2, but with a longer period of 30 months, sharper transitions between easterly and westerly winds, and an asymmetry with stronger easterlies and faster westerlies. The influence of the boundary conditions lasts around three cycles.

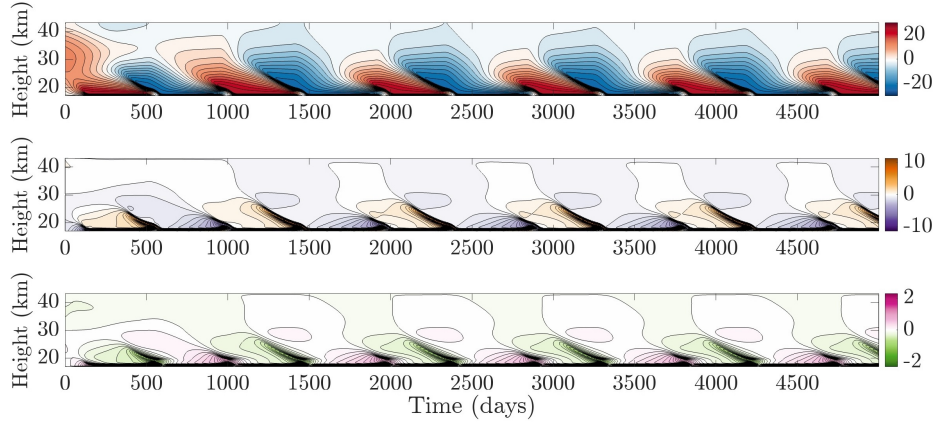


**Fig. 3:** Time-height sections of the QBO zonal-mean wind (m/s), temperature (K) and ozone mixing ratio (ppmv) calculated integrating eqs. (16), (25) and (26) with  $w = 0$  (no upwelling). The period was found to be 29.93 months and the average perturbations were  $-0.75 \pm 10.08$  m/s,  $0.012 \pm 1.850$  K,  $-0.0027 \pm 0.3131$  ppmv respectively.

#### 4.2. OZONE

In this subsection, we will explore through a series of experiments the effect of the ozone feedback on the QBO dynamics. For this purpose, we will take upwelling into consideration, but we will keep  $s_C = 0$  so CO<sub>2</sub> perturbations do not play a role.

**Full QBO.** Figure 4 runs the full QBO simulation. The magnitudes of oscillations in the zonal-mean wind, temperature, and ozone mixing ratio are within what was expected from observations [5, 12, 13] with a slightly high period of 33 months. Again, it takes three cycles for the influence of the boundary conditions to disappear. It also exhibits a phase shift in ozone at 30 km.

**No infrared cooling or radiation absorption.** Figure 3 does not take upwelling into account. That is, the effect of the infrared cooling of temperature anomalies ( $h = 0$ ) and radiation absorption by ozone anomalies ( $s_O = 0$ ) are not present. The percentage change of the average perturbations compared to fig. 4 are: 8.8% decrease in period, 807% decrease in zonal wind, 74% decrease in temperature, 120% decrease in ozone. In particular, the wind asymmetry strengthens (westerly phases weaken, easterly phases propagate slower) and the phase shift in ozone at the upper atmosphere weakens.

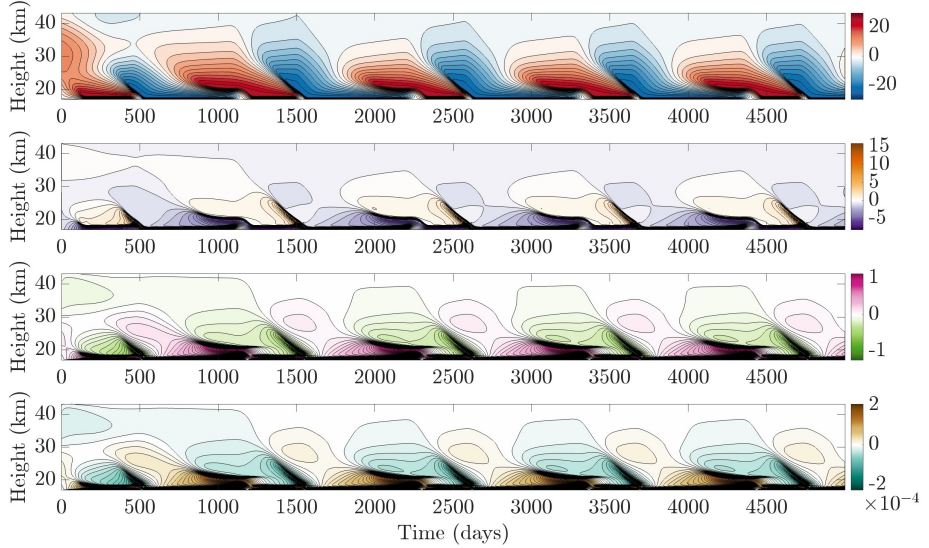


**Fig. 4:** Time-height sections of the QBO zonal-mean wind (m/s), temperature (K), ozone mixing ratio (ppmv) and upwelling (m/s) calculated integrating eqs. (16) and (25) to (27) with  $s_C = 0$  (full simulation). The period of this QBO was found to be 32.81 months and the average perturbations were  $0.11 \pm 9.88$  m/s,  $0.046 \pm 1.942$  K,  $0.011 \pm 0.228$  ppmv,  $(0.22 \pm 4.20) \times 10^{-5}$  m/s respectively.

**No radiation absorption.** Figure 5 does not take the ozone feedback into account. That is, the effect of radiation absorption by ozone anomalies ( $s_O = 0$ ) is not present. The percentage change of the average perturbations compared to fig. 4 are: 8.8% decrease in period, 800% decrease in zonal wind, 72% decrease in temperature, 120% decrease in ozone, 105% decrease in upwelling. Further, the wind asymmetry strengthens and the ozone phase shift in the upper atmosphere weakens. The opposite happens when compared with fig. 3. The zonal wind behaviour at the highest 10 km is very similar to fig. 4. Note that there are some hints of numerical instability in the upwelling graph with unnatural sharp edges.

**No infrared cooling.** Figure 6 does not take thermal wind balance into account. That is, the effect of infrared cooling by temperature anomalies ( $h = 0$ ) is not present. The percentage change of the average perturbations compared to fig. 4 are: 1.1% decrease in period, 69% decrease in zonal wind, 0.49% decrease in temperature, 1.7% increase in ozone, 9.1% decrease in upwelling. Further, compared to both figs. 3 and 4, the wind asymmetry weakens and the phase shift in ozone at the upper atmosphere strengthens. The behaviour at the lower stratosphere is very similar to fig. 4.

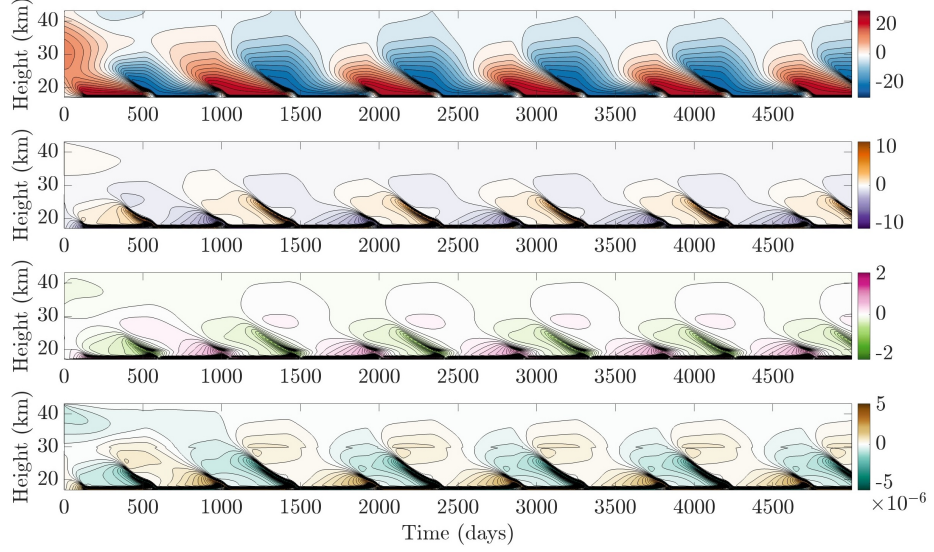


**Fig. 5:** Time-height sections of the QBO component of the zonal-mean wind (m/s), temperature (K), ozone mixing ratio (ppmv) and upwelling (m/s) calculated integrating eqs. (16) and (25) to (27) with  $s_O = 0$ ,  $s_C = 0$  (no radiation absorption). The period was found to be 29.91 months and the average perturbations were  $-0.74 \pm 10.08$  m/s,  $0.013 \pm 1.852$  K,  $-0.0027 \pm 0.3071$  ppmv,  $(-0.10 \pm 1.04) \times 10^{-6}$  m/s respectively.

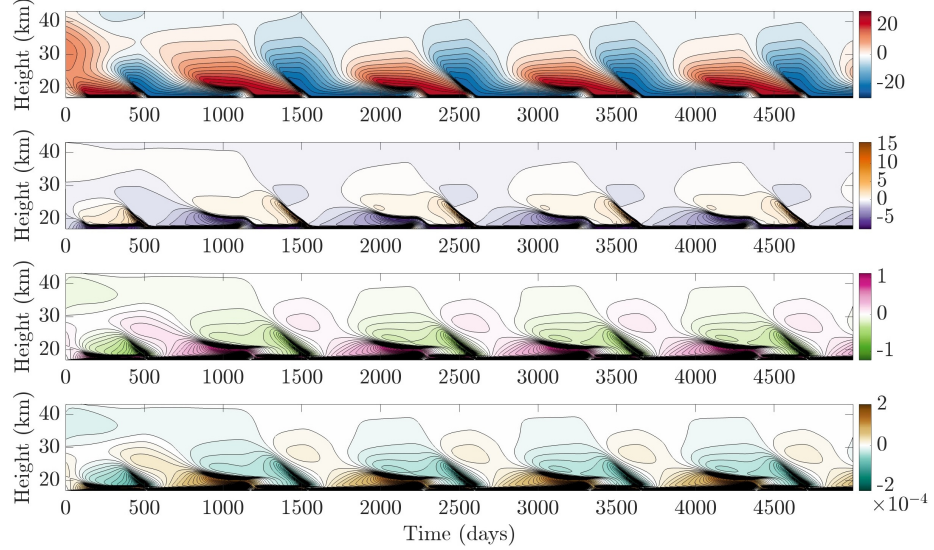


**Fig. 6:** Time-height sections of the QBO component of the zonal-mean wind (m/s), temperature (K), ozone mixing ratio (ppmv) and upwelling (m/s) calculated integrating eqs. (16) and (25) to (27) with  $h = 0$ ,  $s_C = 0$  (no infrared cooling). The period was found to be 32.45 months and the average perturbations were  $0.032 \pm 9.854$  m/s,  $0.045 \pm 1.938$  K,  $0.011 \pm 0.227$  ppmv,  $(0.20 \pm 4.10) \times 10^{-5}$  m/s respectively.

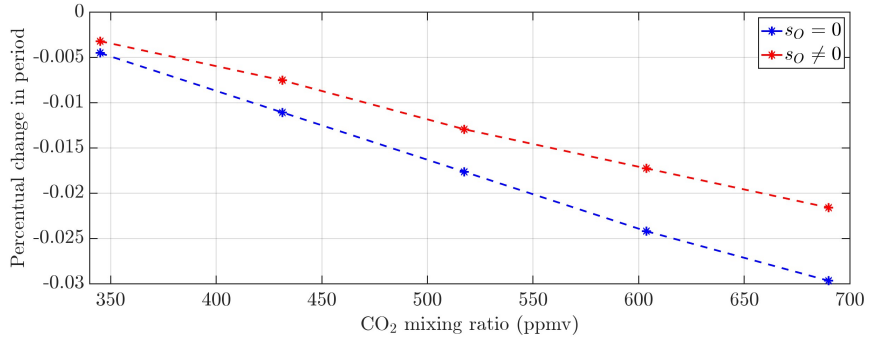


**Fig. 7:** Plot of the percentual change in QBO period with increasing CO<sub>2</sub> mixing ratio for a model with (red) and without (blue) ozone feedback.

#### 4.3. CARBON DIOXIDE

In this subsection, we investigate the impact of rising concentrations of stratospheric CO<sub>2</sub> on QBO dynamics. To do so, we conduct simulations with ( $s_O \neq 0$ ) and without ( $s_O = 0$ ) ozone feedback, using varying levels of CO<sub>2</sub>. We move from the current value of 345 ppmv to twice this quantity, 690 ppmv. Since CO<sub>2</sub> cools the stratosphere, we set its heating coefficient to  $s_C = -1 \times 10^{-7}$ , which is of the same order of magnitude as the aerosol heating coefficient used in [6]. We evaluate the change in the QBO dynamics by comparing the periods obtained with and without ozone feedback with the ones found for figs. 4 and 5 respectively. The results are presented in fig. 7. Clearly, the ozone feedback slows down the change in the QBO period.

## 5 Discussion

### 5.1. QBO MECHANISM

Figure 2 illustrates how the basic characteristics of the QBO can be depicted using a fairly simple model. Figure 3 show how the asymmetry in QBO winds seen in observations [13] can be implemented in the model by considering different attenuation rates for easterly and westerly waves. Moreover, it seems that the extended model is substantially more dependent on the initial conditions. This dependence is partially why there is a slight increase in the period to 30 months, and would be reduced if the simulation ran for longer. Therefore, it would be pertinent to reproduce these results by running longer simulations that minimise the impact of initial conditions in future studies. This is also applicable to the findings discussed in the following subsections.

## 5.2. OZONE

Figures 3 to 6 illustrate the effect of radiation absorption (ozone feedback) and infrared cooling on QBO dynamics.

Firstly, with respect to zonal-mean wind perturbations, we can measure the level of asymmetry between easterly and westerly winds visually or by looking at the average zonal-mean wind (less asymmetry the closest it is to zero). Doing so, we see that this asymmetry is maximised when only radiation absorption is taken into account (fig. 6) and minimised when it is not present (figs. 3 and 5). Therefore, in agreement with [6], the ozone feedback smoothens the wind asymmetry making westerly phases propagate slower and weakening easterly phases.

As expected, the inclusion of radiation absorption leads to a rise in temperature, as illustrated in fig. 4 compared to fig. 5. Conversely, one would expect a decrease in temperature when considering infrared cooling, as shown by the comparison between fig. 4 and fig. 6. However, a subtle increase is observed instead. This anomaly is likely attributed to the fact that an identical number of oscillations were not precisely taken into account in the average and having had reduced  $h$  by two orders of magnitude. This reduction in  $h$  was necessary to prevent the upwelling from becoming too strong for the QBO to form. A possible reason for this could be our omission of the temperature dependence of the attenuation rates in eqs. (12) and (13). Hence, incorporating this temperature dependence could be a valuable area of focus for future research.

Moreover, it appears that zonal-mean ozone and upwelling perturbations are predominantly driven by radiation absorption, particularly in the lower stratosphere. This is evident both visually (fig. 4 resembles fig. 6) and looking at the percentage change between the average ozone and upwelling perturbations in figs. 5 and 6 with respect to fig. 4. This behaviour aligns with the findings of [12], but it might be exaggerated by our choice of  $h$ , which was reduced by two orders of magnitude. Lastly, it's worth noting that the ozone phase shift at 30 km seen in observations [12] is amplified by radiation absorption, as seen when comparing figs. 4 and 6.

The numerical instability observed in fig. 5 raises concerns about the reliability of the model's predictions. Hence, developing a fully-implicit scheme would be of great interest. This would also allow us to take into account the temperature dependence of the attenuation rates as it makes the scheme unstable at the moment.

### 5.3. CARBON DIOXIDE

Figure 7 suggests that the ozone feedback mechanism plays a crucial role in stabilising the time evolution of the QBO in the face of increasing levels of stratospheric carbon dioxide. This is in alignment with the results presented in [6] where a similar effect was found in the face of perturbations by volcanic aerosols. Note, however, that the carbon heating coefficient used ( $s_C = -1 \times 10^{-7}$ ) is just an estimation, so these results are preliminary. Specifically, the percentages shown could vary significantly, but the trends with and without ozone feedback are expected to be of a similar form. If we want to obtain more accurate results, this coefficient must be derived from real data.

## 6 Conclusion

We presented a one-dimensional model of the Quasi-Biennial Oscillation (QBO) with linearised equations of ozone radiation and photochemistry to study the effect of the ozone feedback on the dynamics of the QBO.

We demonstrated how the basic characteristics of the QBO can be replicated using the simple model and how it can be extended to exhibit the observed asymmetries between westerly and easterly winds using the extended model.

We then moved on to explore the effect of coupling the QBO mechanism to linearised equations of ozone radiation and photochemistry. Our analysis revealed that adding this ozone feedback smoothens the asymmetry between westerly and easterly winds, increases the mean zonal temperature, strengthens the ozone phase shift in the upper stratosphere and drives ozone and upwelling perturbations in the lower stratosphere.

Finally, we showed that the ozone feedback mechanisms stabilise the QBO in the face of increasing stratospheric carbon dioxide concentrations by reducing the percentual change in the QBO period as these levels rise.

We also identified several areas for future research: (1) running longer simulations to minimise the impact of initial conditions (2) developing a fully-implicit scheme that would improve the reliability of the model's predictions and allow us to take into consideration the temperature dependence of the attenuation rates (3) estimate  $s_C$  by

fitting it to actual real data in order to obtain more accurate and definite results in relation to stratospheric carbon dioxide.

In conclusion, our project showcased the impacts of adding ozone feedback to the QBO mechanism and highlighted the importance of incorporating it in our climate models to accurately predict QBO dynamics and stability. Additionally, we identified multiple interesting phenomena where further research could be carried out.

## References

- [1] M. Baldwin et al. “The quasi-biennial oscillation”. *Reviews of Geophysics* **39**.2 (2001), pp. 179–229.
- [2] J. A. Anstey et al. “Impacts, processes and projections of the quasi-biennial oscillation”. *Nature Reviews Earth & Environment* **3**.9 (2022), pp. 588–603.
- [3] M. A. Diallo et al. “Stratospheric water vapour and ozone response to the quasi-biennial oscillation disruptions in 2016 and 2020”. *Atmospheric Chemistry and Physics* **22**.21 (2022), pp. 14303–14321.
- [4] K. Rajendran et al. “Synchronisation of the equatorial QBO by the annual cycle in tropical upwelling in a warming climate”. *Quarterly Journal of the Royal Meteorological Society* **142**.695 (2016), pp. 1111–1120.
- [5] X.-D. Ling and J. London. “The quasi-biennial oscillation of ozone in the tropical middle stratosphere: A one-dimensional model”. *Journal of Atmospheric Sciences* **43**.24 (1986), pp. 3122–3137.
- [6] R. Tanii and F. Hasebe. “Ozone feedback stabilizes the quasi-biennial oscillation against volcanic perturbations”. *Geophysical research letters* **29**.7 (2002), pp. 14–1.
- [7] R. Plumb. “The interaction of two internal waves with the mean flow: Implications for the theory of the quasi-biennial oscillation”. *Journal of Atmospheric Sciences* **34**.12 (1977), pp. 1847–1858.
- [8] J. R. Holton and R. S. Lindzen. “An updated theory for the quasi-biennial cycle of the tropical stratosphere”. *Journal of Atmospheric Sciences* **29**.6 (1972), pp. 1076–1080.
- [9] N. Butchart. “The Brewer-Dobson circulation”. *Reviews of Geophysics* **52**.2 (2014), pp. 157–184.
- [10] J. Hampson and P. Haynes. “Phase alignment of the tropical stratospheric QBO in the annual cycle”. *Journal of the atmospheric sciences* **61**.21 (2004), pp. 2627–2637.
- [11] G. K. Vallis. *Essentials of atmospheric and oceanic dynamics*. Cambridge university press, 2019.
- [12] F. Hasebe. “Quasi-Biennial Oscillations of Ozone and Diabatic Circulation in the Equatorial Stratosphere”. *Journal of Atmospheric Sciences* **51**.5 (1994), pp. 729 –745.

- [13] NASA. *The Quasi-biennial Oscillation (QBO)*. 2024. URL: [https://acd-ext.gsfc.nasa.gov/Data\\_services/met/qbo/qbo.html](https://acd-ext.gsfc.nasa.gov/Data_services/met/qbo/qbo.html).

## Appendix A Wave Momentum Deposition

In this section we outline of how the momentum deposition term given in eq. (2) can be derived. We start by modelling the compressible, non-isothermal stratospheric flow  $\mathbf{u}$  using the continuity equation (describing the conservation of mass) and the Navier-Stokes equation (describing the conservation of momentum) for constant viscosity  $\nu$  given by

$$\frac{1}{\rho} \left( \frac{\partial \rho}{\partial t} + (\mathbf{u} \cdot \nabla) \rho \right) + \nabla \cdot \mathbf{u} = 0, \quad (42)$$

$$\rho \left( \frac{\partial \mathbf{u}}{\partial t} + (\mathbf{u} \cdot \nabla) \mathbf{u} \right) = -\nabla p + \nu \nabla^2 \mathbf{u} + \frac{1}{3} \nu \nabla (\nabla \cdot \mathbf{u}) + \rho \mathbf{g}, \quad (43)$$

where  $\rho$  is density and  $\mathbf{g}$  the gravitational acceleration. Since the wave perturbations  $\rho'(\mathbf{x}, t)$  of the average density  $\bar{\rho}(z, t)$  are relatively small, we can perform the Boussinesq approximation to reduce the non-linearity of the problem. This consists of decomposing the density into  $\rho(\mathbf{x}, t) = \bar{\rho}(z) + \rho'(\mathbf{x}, t)$  and assuming that  $\rho'(\mathbf{x}, t)$  is small enough to not affect the flow field, except that it gives rise to buoyancy forces. Hence,  $\rho'(\mathbf{x}, t)$  is accounted for only as part of the buoyancy force  $\sigma = -g\rho'/\bar{\rho}$ . Then, eqs. (42) and (43) become

$$\nabla \cdot \mathbf{u} = 0, \quad (44)$$

$$\left( \frac{\partial \mathbf{u}}{\partial t} + (\mathbf{u} \cdot \nabla) \mathbf{u} \right) = -\frac{\nabla p}{\bar{\rho}} + \frac{\nu \nabla^2 \mathbf{u}}{\bar{\rho}} + \frac{(\bar{\rho} + \rho')}{\bar{\rho}} g, \quad (45)$$

Restricting ourselves to 2D motion in the xz-plane, since the flow is incompressible to first order ( $\nabla \cdot \mathbf{u}(\mathbf{x}, t) = 0$ ) then we can describe the wind flow as the derivative of a (stream)function  $\psi$  such that  $\mathbf{u} = (v, 0, u) = (\partial_z \psi, 0, -\partial_x \psi)$ . Then, the dynamics of the flow are governed by two coupled equations. Firstly, taking the curl<sup>3</sup> of eq. (45) we obtain the vorticity equation

$$\frac{\partial \mathbf{w}}{\partial t} - \nu \nabla^2 \mathbf{w} - \nabla \frac{\rho'}{\bar{\rho}} \mathbf{g} = (\mathbf{w} \cdot \nabla) \mathbf{u} - (\mathbf{u} \cdot \nabla) \mathbf{w}, \quad (46)$$

---

<sup>3</sup>It is helpful to remember the following identities for any vectors  $\mathbf{a}$ ,  $\mathbf{b}$  or scalar  $c$  (1)  $\nabla \times \nabla c = 0$  (2)  $\frac{1}{2} \nabla(\mathbf{a} \cdot \mathbf{a}) = (\mathbf{a} \cdot \nabla) \mathbf{a} + \mathbf{a} \times (\nabla \times \mathbf{a})$  (3)  $\nabla \times (\mathbf{a} \times \mathbf{b}) = (\mathbf{b} \cdot \nabla) \mathbf{a} - (\mathbf{a} \cdot \nabla) \mathbf{b} + \mathbf{a}(\nabla \cdot \mathbf{b}) - \mathbf{b}(\nabla \cdot \mathbf{a})$ .

where  $\mathbf{w} = \nabla \times \mathbf{u}$ , or in terms of the stream function (y-component of eq. (46))

$$\frac{\partial(\nabla^2\psi)}{\partial t} - v\nabla^4\psi + \frac{\partial\sigma}{\partial x} = J(\psi, \nabla^2\psi) \quad (47)$$

where the jacobian is defined as  $J(a, b) = \partial_x a \partial_z b - \partial_z a \partial_x b$ . Secondly, we can close the system by stating, following [7], that the buoyancy is governed by

$$\frac{\partial\sigma}{\partial t} - N^2 \frac{\partial\psi}{\partial x} + \mu\sigma = J(\psi, \sigma) \quad (48)$$

where  $N$  is the buoyancy frequency defined by  $N^2(z) = -(g/\bar{\rho})\partial_z\bar{\rho}$  and  $\mu$  is the thermal dissipation rate. If we now decompose  $\psi = \bar{\psi}(z) + \psi'(\mathbf{x}, t)$  and only retain first-order disturbance quantities we obtain the following vorticity equation

$$\frac{\partial}{\partial t} \left( \frac{\partial \bar{u}}{\partial z} + \nabla^2 \psi' \right) - v \nabla^4 (\bar{\psi} + \psi') + \frac{\partial\sigma}{\partial x} = \frac{\partial\psi'}{\partial x} \frac{\partial^2 \bar{u}}{\partial z^2} - \bar{u} \frac{\partial}{\partial x} \nabla^2 \psi', \quad (49)$$

where we used  $\bar{u} = \partial_z \bar{\psi}$ . Similarly, the decomposition applied to the buoyancy equation gives

$$\frac{\partial\sigma}{\partial t} - N^2 \frac{\partial\psi'}{\partial x} + \mu\sigma = -\bar{u} \frac{\partial\sigma}{\partial x}. \quad (50)$$

Assuming that we can neglect viscous dissipation of the wave (less effective than thermal dissipation) and that the time-scale of changes in the mean flow are much larger than those of wave motion, we neglect terms with  $\partial\bar{u}/\partial t$ , it can be shown [7] that the system of eqs. (49) and (50) admits plane wave solutions of the form

$$\psi'_n = \text{Re} \left[ \tilde{\psi}_n e^{ik_n(x - c_n t)} \right], \quad (51)$$

satisfying

$$\frac{\partial^2 \tilde{\psi}_n}{\partial z^2} + \left[ \frac{N^2(1 + \frac{i\mu}{k(\bar{u} - c_n)})}{(\bar{u} - c_n)^2 + \frac{\mu^2}{k_n^2}} - k_n^2 - \frac{1}{\bar{u} - c_n} \frac{\partial^2 \bar{u}}{\partial z^2} \right] \tilde{\psi}_n = 0. \quad (52)$$

where  $\tilde{\psi}_n$ ,  $k_n$ , and  $c_n$  are the amplitude, wave number and horizontal phase speed of the nth wave respectively.

To simplify we further assume that  $\mu \ll k_n(\bar{u} - c_n)$  so we can neglect  $\mu^2/k_n^2$ , that the vertical length-scale  $D$  is much smaller than the horizontal length-scale  $L$  so  $D/L \ll 1$  and we can neglect  $k_n^2$ , and that  $\partial_z \bar{u} \ll N^2$  so we can neglect the  $\partial_z^2 \bar{u}$  term.

Hence, we find

$$\frac{\partial^2 \tilde{\psi}_n}{\partial z^2} + m(z)^2 \tilde{\psi}_n = 0, \quad (53)$$

with

$$m_n(z) = \left[ \frac{N^2(1 + \frac{i\mu}{k(\bar{u}-c_n)})}{(\bar{u}-c_n)^2} \right]^{1/2} \simeq \frac{N^2}{(\bar{u}-c_n)^2} \left[ 1 + \frac{i\mu}{2k(\bar{u}-c_n)} \right]. \quad (54)$$

whose WKB solution representing an upward propagating wave is

$$\tilde{\psi}_n(z) = A m_n(z)^{-1/2} \exp \left( i \int^z m_n(z') dz' \right) \quad (55)$$

where  $A$  is an arbitrary constant set by the boundary conditions and we have assumed that the vertical group velocity of the wave is positive (otherwise the exponential would be negative). The horizontal momentum flux associated with this wave is then

$$\begin{aligned} F_n(z, t) &= \overline{u'_n v'_n} = -\frac{k_n}{2} \operatorname{Re} \left[ i \frac{\partial \tilde{\psi}_n}{\partial z} \tilde{\psi}_n^* \right] = -\frac{ik_n}{4} \left( \tilde{\psi}_n \frac{\partial \tilde{\psi}_n^*}{\partial z} - \tilde{\psi}_n^* \frac{\partial \tilde{\psi}_n}{\partial z} \right) \\ &= F_n(z_l) \exp \left( - \int_{z_l}^z \frac{N\mu}{k_n(\bar{u}(z', t) - c_n)} dz' \right), \end{aligned} \quad (56)$$

where the asterisk means conjugate transpose.

## Appendix B Matlab Implementation

```

1 %% Define mesh (spatial)
2
3 eta_l = 0; % lower boundary
4 eta_t = 4; % top boundary
5 J = 100; % number of grid points
6 deta = (eta_t-eta_l)/(J); % vertical step
7 eta = linspace(eta_l,eta_t,J); % vertical grid points
8
9 %% Constants and dimensions
10
11 % Dimensional constants
12 kappa_dim = 0.3; %m^2s^-1
13 F_dim = 16e-3; %m^2s^-2
14 N_dim = 2.16e-2; %s^-1
15 mu_dim = 1e-6; %s^-1
16 k_dim = 2*pi/(40e6); %m^-1
17 c_dim = 30; %m/s
18
19 H = 7000; %m
20 Omega = 7.27e-5; % rad/s
21 a = 6.371e6; % m

```

```

22 beta_dim = 2*Omega/a; % s^-1
23
24 chi_dim = 10; %ppmv
25 L = 1e6; % m
26 R = 287; % m^2 s^-2 K^-1
27 h = @(j) (5.4e-7*(1+(2/3)*j*data).*(j*data<=1.99)+1.56e-6.* (j*data>1.99))/100; % s^-1
28 gamma_0 = -2.24e-7; % s^-1
29 gamma_T = -1.24e-12*1e6; % m^-1 s
30 s_0 = 8.39e-2*1e-6; % m s^-3
31 s_C = 0; %-1e-7*1e-6; % m s^-3
32
33 % Dimensionless constants
34 alpha = @(j) (0.55+0.55*(j*data)).*(j*data<=1.99)+1.65.* (j*data>1.99);
35 Lambda = kappa_dim*N_dim*mu_dim/(k_dim*c_dim*F_dim);
36 eps = N_dim*mu_dim/(H*k_dim*c_dim^2);
37 beta = beta_dim/(k_dim^2*c_dim);
38 theta = 2*pi*k_dim*c_dim^3/(360*N_dim*mu_dim*F_dim);
39
40 Gamma_0 = gamma_0*k_dim*c_dim^3/(mu_dim*F_dim*N_dim);
41 Gamma_T = gamma_T*L^2*Omega*c_dim^2/(a*F_dim*chi_dim);
42
43 Xi = @(j) h(j)*L^2*Omega*mu_dim/(a*k_dim*F_dim*N_dim);
44 S_0 = s_0*c_dim*chi_dim/(F_dim*N_dim^2);
45 S_C = s_C*c_dim*chi_dim/(F_dim*N_dim^2);
46
47 % Dimensionless variables
48 zz = @(eta) eta*(k_dim*c_dim^2/(N_dim*mu_dim*1000))+17; %km
49 tt = @(xi) xi*(k_dim*c_dim^3/(N_dim*mu_dim*F_dim*3600*24)); % days
50 uu = @(u) c_dim*u; % m/s
51 TT = @(T) L^2*Omega*H*N_dim*mu_dim/(R*a*k_dim*c_dim)*T; % K
52 cchi = @(chi) chi_dim*chi; % ppv m^-1
53
54 %% Define time step
55
56 dt = 0.05; % days time step
57 dxi = dt*(3600*24)*(N_dim*mu_dim*F_dim)/(k_dim*c_dim^3); % convert
58 N = 99999; % # timesteps
59 xi = 0:dxi:dxi*N; % time array
60
61 %% Initialise arrays
62
63 u = zeros(length(eta),N+1); % mean wind array
64 T = zeros(length(eta),N+1); % temperature array
65 chi_0 = zeros(length(eta),N+1); % mixing ratio array
66 w = zeros(length(eta),N+1); % upwelling array
67
68 % initial states
69 u(:,1) = 0.5*sin(pi*eta/4);
70 T(:,1) = 0.5*(pi/4)*cos(pi*eta/4);
71 chi_0(:,1) = 0.01*sin(pi*eta/2);
72 w(:,1) = -Xi(1:J).*T(1:J,1)+S_0*chi_0(1:J,1);
73
74 %% Define terms in equation
75

```

```

76 F_OK = 1; F_ORG = -1; % wave momentum flux
77 c_K = 1; c_RG = -1; % ms^-1 wavespeeds
78 k_K = 1; k_RG = 3; % km^-1 wavenumber
79
80 g_K = @(u,j,jj,n) alpha(j)./(k_K.* (u(jj,n)-c_K).^2); % rate of decay
81 g_RG = @(u,j,jj,n) alpha(j)./(k_RG.* (u(jj,n)-c_RG).^2).* (beta./(k_RG.^2.* (u(jj,n)-c_RG
    ))-1); % rate of decay
82
83 F_K = @(u,j,n) F_OK.*exp(-trapz(g_K(u,j,1:j,n))*deta); % wave momentum flux
84 dF_K = @(u,j,n) -F_K(u,j,n).*g_K(u,j,j,n); % wave momentum flux derivative
85
86 F_RG = @(u,j,n) F_ORG.*exp(-trapz(g_RG(u,j,1:j,n))*deta); % wave momentum flux
87 dF_RG = @(u,j,n) -F_RG(u,j,n).*g_RG(u,j,j,n); % wave momentum flux derivative
88
89 G = @(u,j,n) -exp(eps*deta*j)*(dF_K(u,j,n)+dF_RG(u,j,n)); % forcing term
90
91 chi_V = 345/chi_dim;
92
93 %% Time stepping
94
95 % Iterate
96 my_waitbar = waitbar(0,'Calculating QBO... (0%)');
97 for n = 2:N
98
99     % Update u
100    a_0 = @(j) 1 + 2*Lambda*dx/deta^2 + w(j,n-1)*dx/deta;
101    a_m1 = @(j) - Lambda*dx/deta^2 - w(j,n-1)*dx/deta;
102    a_p1 = - Lambda*dx/(deta)^2;
103    a_LHS = diag(a_0(2:J-1),0) + diag(a_m1(3:J-1),-1) + diag(a_p1*ones(1,J-3),1);
104
105    GG = arrayfun(@(j)G(u,j,(n-1))*(abs(G(u,j,(n-1)))<100)+100*(abs(G(u,j,(n-1)))
106        >=100),2:J-1)';
107    a_RHS = u(2:J-1,n-1) + dx*GG;
108
109    a_LHS = cat(2,[a_m1(2) zeros(1,J-3)]',a_LHS,[zeros(1,J-3) a_p1]');
110    a_LHS = cat(1,[1 zeros(1,J-1)],a_LHS,[zeros(1,J-3) 1 -4 3]); % BC LHS
111    a_RHS = cat(1,0,a_RHS,0); % BC RHS
112
113    u(1:J,n) = a_LHS\ a_RHS;
114
115    % Update T
116    T(1,n) = - (-3*u(1,n)+4*u(2,n)-u(3,n))/(2*deta);
117    T(2:J-1,n) = - (u(3:J,n)-u(1:J-2,n))/(2*deta);
118    T(J,n) = - (u(J-2,n)-4*u(J-1,n)+3*u(J,n))/(2*deta);
119
120    % Update chi
121    b_0 = @(j) 1 + w(j,n-1).*dx/deta.*(w(j,n-1)>=0) - w(j,n-1).*dx/deta.*(w(j,n-1)
122        <0) - dx*Gamma_0;
123    b_m1 = @(j) - w(j,n-1).*dx/deta.*(w(j,n-1)>=0); % if w>0 backwards difference
124    b_p1 = @(j) w(j,n-1).*dx/deta.*(w(j,n-1)<0); % if w<0 forwards difference
125
126    b_LHS = diag(b_0(2:J-1),0)+diag(b_m1(3:J-1),-1)+diag(b_p1(2:J-2),1);
127    b_LHS = cat(2,[b_m1(2) zeros(1,J-3)]',b_LHS,[zeros(1,J-3) b_p1(J-1)]');
128    b_RHS = chi_0(2:J-1,n-1)+dx*Gamma_T*T(2:J-1,n);

```

```

127
128 if w(1,n-1) > 0 % BC needed at the beginning
129     b_LHS = cat(1,[1 zeros(1,J-1)],b_LHS);
130     b_RHS = cat(1,0,b_RHS);
131 else % Point calculated using explicit forward differences
132     b_LHS = cat(1,[b_0(1) b_p1(1) zeros(1,J-2)],b_LHS);
133     b_RHS = cat(1,chi_0(J,n-1)+dxi*Gamma_T*T(J,n),b_RHS);
134 end
135
136 if w(J,n-1) < 0 % BC needed at the end
137     b_LHS = cat(1,b_LHS,[zeros(1,J-3) 1 -4 3]);
138     b_RHS = cat(1,b_RHS,0);
139 else % Point calculated using implicit backwards differences
140     b_LHS = cat(1,b_LHS,[zeros(1,J-2) b_m1(J-1) b_0(J)]);
141     b_RHS = cat(1,b_RHS,chi_0(J,n-1)+dxi*Gamma_T*T(J,n));
142 end
143
144 chi_0(1:J,n) = b_LHS\b_RHS;
145
146 % Update w
147 w(1:J,n) = -Xi(1:J).*T(1:J,n)+S_0*chi_0(1:J,n)+S_C*chi_V*ones(J,1);
148
149 % Update waitbar
150 waitbar(n/(N-2),my_waitbar,sprintf('Calculating QBO... (Percentage done: %3.3f )',
151 ,n/(N-2)*100))
152 end
153 %% Find period at height 24km
154
155 eta_eval = int64((24-17)*(N_dim*mu_dim*1000)/(k_dim*c_dim^2)); % eta corresponding to
156 % 24km
157 s = u(eta_eval/deta,:); % zonal mean flow at 24km
158 [ac,lags] = xcorr(s,s); % autocorrelation function
159 locs = islocalmax(ac); % find peaks
160 period = tt(mean(diff(lags(locs)*dxi))/30.4167; % period in months
161
162 %% Save averages
163 fileID = fopen('results.txt','w');
164 fprintf(fileID,'%12s %12s %12s\n','var','mean','std');
165 fprintf(fileID,'%12s %12f %12f\n','period', period,0);
166 fprintf(fileID,'%12s %12f %12f\n','u', mean(uu(u(:))), std(uu(u(:))));
167 fprintf(fileID,'%12s %12f %12f\n','T', mean(TT(T(:))), std(TT(T(:))));
168 fprintf(fileID,'%12s %12f %12f\n','chi', mean(cchi(chi_0(:))), std(cchi(chi_0(:))));
169 fprintf(fileID,'%12s %12f %12f\n','w', mean(w(:)*F_dim/c_dim), std(w(:)*F_dim/c_dim));
170 fclose(fileID);

```